

A New CAA Formulation based on Lighthill's Analogy applied to an Idealized Automotive HVAC Blower using AcuSolve and ACTRAN/LA

Stéphane Caro*, Paul Ploumhans, Xavier Gallez *Free Field Technologies SA* – fft.be
16 place de l'Université, B1348 Louvain-la-Neuve, Belgium

Robert Sandboge, *Simmetrix, Inc.* – simmetrix.com
10 Halfmoon Executive Park Drive, Clifton Park, NY 12065, USA

Farzin Shakib, *ACUSIM Software, Inc.* – acusim.com
2685 Marine Way, Suite 1215, Mountain View, California 94043, USA

Marcus Matthes, *Visteon GmbH* – visteon.com
Visteon European Corporate Office and Innovation Center, Visteonstrasse 4-10, 50170 Kerpen, Germany

In this paper, we investigate the use of the variational formulation of Lighthill's analogy, implemented in a Finite/Infinite Element framework. We present an innovative way to handle porous boundaries (or equivalently, control surfaces upon which aerodynamic sources are defined). We show how Lighthill's analogy can be used to predict broadband blower noise. Infinite elements are used to enforce the Sommerfeld radiation boundary condition.

A derivation of the analogy is presented and is compared with the derivation of Curle's analogy (extended to handle porous boundaries). The implementation is described and is validated on a test case. Preliminary results on a real automotive HVAC blower case are presented.

*Corresponding author: stephane.caro@fft.be

Copyright © 2005 by Free Field Technologies SA. Published by the American Institute of Aeronautics and Astronautics, Inc. with permission.

Nomenclature

Latin symbols

a_0	Speed of sound at rest
\mathbf{divT}	Divergence of the Lighthill's tensor \mathbf{T} , $divT_i = \partial T_{ij} / \partial x_j$
f	Frequency
k	Wavenumber $k = \omega / a_0$
M	Mach number
p	Pressure
r	Distance from the source to the observer, $r = \mathbf{x} - \mathbf{y} $
Re	Reynolds number
\mathbf{b}	Body force
t	Time
t'	Retarded time, $t' = t - r / a_0$
\mathbf{T}	Lighthill stress tensor
\mathbf{v}	Fluid velocity vector
\mathbf{x}	Position of the observer
\mathbf{y}	Position of the source

Greek symbols

δ	Identity matrix
γ	Ratio of specific heats
λ	Acoustic wavelength, $\lambda = a_0 / f$
ω	Reduced frequency, $\omega = 2\pi f$
ρ	Fluid density
ρ_0	Fluid density in fluid at rest
ρ_a	Acoustic density fluctuation
Σ	Divergence of total stress
τ	Viscous stress tensor
τ_c	Least-square metric (cont. eq.)
τ_m	Least-square metric (mom. eq.)

Notations

\mathbf{z}	Vector $\mathbf{z} = \begin{pmatrix} z_1 \\ \vdots \\ z_m \end{pmatrix}$
z_n	Normal component of vector \mathbf{z} , $\mathbf{v} \cdot \mathbf{n}$
\tilde{z}	Fourier-transform of the variable z

I. Introduction

The purpose of this work is to evaluate a Computer Aided Engineering (CAE) method in which computational aero acoustics (CAA) techniques are used to predict the noise level from an automotive blower. The engineering objective is to ensure that the noise level in an automotive air handling system is sufficiently low for all operating conditions. In fact, automobile manufacturers are placing increased emphasis on the reduction of passenger compartment noise level so that this noise reduction has become a critical design consideration. This has resulted in more stringent noise requirements for air handling systems. For most operating conditions, the blower is the major noise contributor. Consequently, significant effort is often spent during product development to reduce the blower noise level. In the past this was usually accomplished through tedious physical testing.

In this paper we present a novel aeroacoustic approach to predict the noise from blowers. This approach is an extension of the variational formulation of Lighthill's analogy, initially proposed by Oberai *et al.*,^{1,2} and also presented in Caro *et al.*³ Such an approach is especially well adapted to treat interior, or ducted, noise problems. To treat blower problems, the new approach makes use of acoustic sources defined both in a volume and on control surfaces which enclose the rotating parts of the blower. The effect of the rotating parts is included in the acoustic calculations through a source term defined on the control surfaces

We also investigate the use of CFD simulations for the determination of the acoustic source terms. Although the acoustic field is truly based on compressible waves, the unsteady flow patterns, i.e., the acoustic source terms, can be adequately represented by a pseudo-compressible flow solution. Note that the acoustic wave propagation predicted by most Navier-Stokes flow solvers (including the solutions obtained here) are not sufficiently accurate to predict sound pressure level at a distance directly, therefore the "noise" must be propagated by an auxiliary method. In other words, the flow solution predicts the source terms, but not sound propagation, well enough.

In this effort, CFD and CAA simulations are done using two commercial codes, ACUSOLVE^{4,5}- CFD code developed by ACUSIM Software Inc. - and ACTRAN/LA⁶ - CAA code developed by Free Field Technologies S.A. - respectively. ACUSOLVE can use an incompressible, pseudo-compressible or compressible formulation. ACTRAN/LA can use aerodynamic sources extracted from ACUSOLVE results. The coupling between ACTRAN/LA and ACUSOLVE is part of a Simulation Based Design (SBD) process proposed by Simmetrix Inc.

II. Proposed formulation

The formulation of ACTRAN/LA is based on Lighthill's acoustic analogy, implemented in its variational form, following the approach first proposed by Oberai *et al.*¹ Moving walls, if any, are assumed to lie outside the computational domain, Ω .

A. Lighthill's analogy

The mass and momentum conservation equations governing the motion of a fluid under no external forces can be written

$$\frac{\partial \rho}{\partial t} + \frac{\partial}{\partial x_i}(\rho v_i) = 0 \quad (1)$$

$$\frac{\partial}{\partial t}(\rho v_i) + \frac{\partial}{\partial x_j}(\rho v_i v_j) = -\frac{\partial p}{\partial x_i} + \frac{\partial \tau_{ij}}{\partial x_j}, \quad (2)$$

where ρ is the fluid density, \mathbf{v} is the velocity, p is the pressure and $\boldsymbol{\tau}$ is the viscous stress tensor. By combination of Eqs. (1) and (2), Lighthill's analogy⁷ is found as

$$\frac{\partial^2}{\partial t^2}(\rho - \rho_0) - a_0^2 \frac{\partial^2}{\partial x_i \partial x_i}(\rho - \rho_0) = \frac{\partial^2 T_{ij}}{\partial x_i \partial x_j}, \quad (3)$$

where ρ_0 denotes the density at rest, a_0 the speed of sound at rest and \mathbf{T} is Lighthill's tensor defined as

$$T_{ij} = \rho v_i v_j + ((p - p_0) - a_0^2(\rho - \rho_0)) \delta_{ij} - \tau_{ij}. \quad (4)$$

For a Stokesian perfect gas like air, in an isentropic, high Reynolds number and low Mach number flow, Lighthill's tensor \mathbf{T} is often approximated by

$$T_{ij} \simeq \rho_0 v_i v_j. \quad (5)$$

Away from the source region, the density fluctuations, $\rho - \rho_0$, correspond to acoustic density fluctuations. This is highlighted by rewriting Eq. (3) as

$$\frac{\partial^2 \rho_a}{\partial t^2} - a_0^2 \frac{\partial^2 \rho_a}{\partial x_i \partial x_i} = \frac{\partial^2 T_{ij}}{\partial x_i \partial x_j}, \quad (6)$$

where $\rho_a = \rho - \rho_0$. Additional details can be found *e.g.* in Lighthill⁷ or Goldstein.⁸

In practice, to use Lighthill's analogy in the two steps procedure described above, one considers that there is no aeroacoustic coupling, *i.e.*, that the influence of the acoustics on the flow is weak. As a result, Lighthill's tensor (*i.e.* the right hand side of Eq. (3)) is considered to be independent from the density fluctuation, $\rho - \rho_0$. This makes Eq. (3) a true wave equation.

The present approach to treat aeroacoustic problems is intended to be used for isentropic flows where the convection and refraction effects can be neglected with respect to the other effects, which is generally true if the Mach number is low enough (below 0.2 - 0.3). Some studies on the flow convection effects at such Mach numbers can be found *e.g.* in Jacob.⁹

B. Integral formulation of Lighthill's analogy

The integral formulation of Lighthill's analogy was first derived by Curle,¹⁰ and is best known as Curle's analogy. The main steps of his developments are reproduced here to allow an easier comparison with the developments of the variational formulation of Lighthill's analogy that will be presented in Section C.

The wave equation (3) can be rewritten in its integral form (Stratton¹¹),

$$\rho - \rho_0 = \frac{1}{4\pi a_0^2} \int_{\Omega} \left[\frac{\partial^2 T_{ij}}{\partial x_i \partial x_j} \frac{1}{r} \right]_{t'} d\mathbf{y} + \frac{1}{4\pi} \int_{\Gamma} \left[\frac{1}{r} \frac{\partial}{\partial n} (\rho - \rho_0) + \frac{1}{r^2} \frac{\partial r}{\partial n} (\rho - \rho_0) + \frac{1}{a_0 r} \frac{\partial r}{\partial n} \frac{\partial}{\partial t} (\rho - \rho_0) \right]_{t'} d\mathbf{y}, \quad (7)$$

where Γ denotes the boundary of the acoustic domain, $r = |\mathbf{x} - \mathbf{y}|$, and the integrals' arguments are evaluated at the retarded time $t' = t - r/a_0$. Starting from this equation, Curle transforms the right-hand side by

integrating the volume integral by parts using Green's theorem twice, and applies some transformations to the surface integral to obtain

$$\begin{aligned} \rho - \rho_0 &= \frac{1}{4\pi a_0^2} \frac{\partial^2}{\partial x_i \partial x_j} \int_{\Omega} \left[\frac{T_{ij}}{r} \right]_{t'} d\mathbf{y} + \frac{1}{4\pi a_0^2} \int_{\Gamma} \left[n_i \frac{1}{r} \frac{\partial}{\partial y_j} \left(T_{ij} + a_0^2 (\rho - \rho_0) \delta_{ij} \right) \right]_{t'} d\mathbf{y} \\ &+ \frac{1}{4\pi a_0^2} \frac{\partial}{\partial x_i} \int_{\Gamma} \left[n_j \frac{1}{r} \left(T_{ij} + a_0^2 (\rho - \rho_0) \delta_{ij} \right) \right]_{t'} d\mathbf{y} . \end{aligned} \quad (8)$$

By substituting for T_{ij} as given by Eq. (4), this becomes

$$\begin{aligned} \rho - \rho_0 &= \frac{1}{4\pi a_0^2} \frac{\partial^2}{\partial x_i \partial x_j} \int_{\Omega} \left[\frac{T_{ij}}{r} \right]_{t'} d\mathbf{y} + \frac{1}{4\pi a_0^2} \int_{\Gamma} \left[n_i \frac{1}{r} \frac{\partial}{\partial y_j} \left(\rho v_i v_j + (p - p_0) \delta_{ij} - \tau_{ij} \right) \right]_{t'} d\mathbf{y} \\ &+ \frac{1}{4\pi a_0^2} \frac{\partial}{\partial x_i} \int_{\Gamma} \left[n_j \frac{1}{r} \left(\rho v_i v_j + (p - p_0) \delta_{ij} - \tau_{ij} \right) \right]_{t'} d\mathbf{y} . \end{aligned} \quad (9)$$

From the momentum conservation equation (2), we have that

$$n_i \frac{\partial}{\partial y_j} \left(\rho v_i v_j + (p - p_0) \delta_{ij} - \tau_{ij} \right) = -n_i \frac{\partial}{\partial t} \left(\rho v_i \right) . \quad (10)$$

Let us first consider the case where each surface is fixed or vibrating in its own plane,

$$v_n = v_i n_i = 0 . \quad (11)$$

Equation (9) then reduces to

$$\rho - \rho_0 = \frac{1}{4\pi a_0^2} \frac{\partial^2}{\partial x_i \partial x_j} \int_{\Omega} \frac{T_{ij} \left(\mathbf{y}, t - \frac{r}{a_0} \right)}{r} d\mathbf{y} + \frac{1}{4\pi a_0^2} \frac{\partial}{\partial x_i} \int_{\Gamma} \frac{P_i \left(\mathbf{y}, t - \frac{r}{a_0} \right)}{r} d\mathbf{y} , \quad (12)$$

with

$$P_i = \left(p \delta_{ij} - \tau_{ij} \right) n_j , \quad (13)$$

where \mathbf{P} is the force per unit area exerted by the fluid on the solid boundaries. Equation (12) is known as *Curle's analogy* (it could also be termed the integral formulation of Lighthill's analogy) and highlights the influence of solid boundaries upon aerodynamic sound: *...one can look upon the sound field as the sum of that generated by a volume distribution of quadrupoles and by a surface distribution of dipoles.*¹⁰ The strength of the dipole per unit area is exactly equal to the force per unit area exerted by the fluid on the solid boundaries.

Now, let us consider the case where each surface is fixed, but porous. This means that the normal to the surface does not vary with time, but that the normal velocity does not vanish on the surface. If we rewrite Eq. (9) using Eq. (10), we obtain

$$\begin{aligned} \rho - \rho_0 &= \frac{1}{4\pi a_0^2} \frac{\partial^2}{\partial x_i \partial x_j} \int_{\Omega} \left[\frac{T_{ij}}{r} \right]_{t'} d\mathbf{y} + \frac{1}{4\pi a_0^2} \frac{\partial}{\partial x_i} \int_{\Gamma} \left[n_j \frac{1}{r} \left(\rho v_i v_j + (p - p_0) \delta_{ij} - \tau_{ij} \right) \right]_{t'} d\mathbf{y} \\ &- \frac{1}{4\pi a_0^2} \int_{\Gamma} \left[n_i \frac{1}{r} \frac{\partial}{\partial t} \left(\rho v_i \right) \right]_{t'} d\mathbf{y} . \end{aligned} \quad (14)$$

Compared to Eq. (12), the dipole term (i.e., the second term on the right-hand side) now includes an additional subterm; moreover, a monopole source term (i.e., third term on the right-hand side) is now also present.

C. Variational formulation of Lighthill's analogy

The variational formulation of Lighthill's analogy was first derived by Oberai^{1,2} *et al.* The strong variational statement associated to Eq. (3) can be written:

$$\int_{\Omega} \left(\frac{\partial^2}{\partial t^2} (\rho - \rho_0) - a_0^2 \frac{\partial^2}{\partial x_i \partial x_i} (\rho - \rho_0) - \frac{\partial^2 T_{ij}}{\partial x_i \partial x_j} \right) \delta \rho \, d\mathbf{x} = 0 \quad \forall \delta \rho \quad (15)$$

where $\delta \rho$ is a test function. The spatial derivatives are integrated by parts using Green's theorem, to obtain the weak variational form:

$$\int_{\Omega} \left(\frac{\partial^2}{\partial t^2} (\rho - \rho_0) \delta \rho + a_0^2 \frac{\partial}{\partial x_i} (\rho - \rho_0) \frac{\partial \delta \rho}{\partial x_i} + \frac{\partial T_{ij}}{\partial x_j} \frac{\partial \delta \rho}{\partial x_i} \right) d\mathbf{x} = \int_{\Gamma} \left(a_0^2 \frac{\partial}{\partial x_i} (\rho - \rho_0) n_i + \frac{\partial T_{ij}}{\partial x_j} n_i \right) \delta \rho \, d\mathbf{x} . \quad (16)$$

By substituting the right hand side of Eq. (4) for T_{ij} in the surface integral, Eq. (16) becomes

$$\int_{\Omega} \left(\frac{\partial^2}{\partial t^2} (\rho - \rho_0) \delta \rho + a_0^2 \frac{\partial}{\partial x_i} (\rho - \rho_0) \frac{\partial \delta \rho}{\partial x_i} + \frac{\partial T_{ij}}{\partial x_j} \frac{\partial \delta \rho}{\partial x_i} \right) d\mathbf{x} = \int_{\Gamma} \frac{\partial}{\partial x_j} (\rho v_i v_j + (p - p_0) \delta_{ij} - \tau_{ij}) n_i \delta \rho \, d\mathbf{x} . \quad (17)$$

If we define the total stress tensor

$$\Sigma_{ij} = \rho v_i v_j + (p - p_0) \delta_{ij} - \tau_{ij} , \quad (18)$$

Eq. (17) becomes:

$$\int_{\Omega} \left(\frac{\partial^2}{\partial t^2} (\rho - \rho_0) \delta \rho + a_0^2 \frac{\partial}{\partial x_i} (\rho - \rho_0) \frac{\partial \delta \rho}{\partial x_i} \right) d\mathbf{x} = - \int_{\Omega} \frac{\partial T_{ij}}{\partial x_j} \frac{\partial \delta \rho}{\partial x_i} d\mathbf{x} + \int_{\Gamma} \frac{\partial \Sigma_{ij}}{\partial x_j} n_i \delta \rho \, d\mathbf{x} . \quad (19)$$

This is the variational formulation of Lighthill's analogy. There are two aerodynamic source terms on the right hand side: a volume term, and a surface term. From the momentum conservation equation (2), we have two possibilities to compute $\partial \Sigma_{ij} / \partial x_j$,

$$n_i \frac{\partial \Sigma_{ij}}{\partial x_j} = n_i \frac{\partial}{\partial x_j} (\rho v_i v_j + (p - p_0) \delta_{ij} - \tau_{ij}) \quad (20)$$

$$= -n_i \frac{\partial}{\partial t} (\rho v_i) . \quad (21)$$

In practical the present work, we have used Eq. (20).

D. Comparison of the integral and variational formulations of Lighthill's analogy

From Section B and C, it is seen that the developments of the integral formulation of Lighthill's analogy (*i.e.* Curle's analogy) and of the variational formulation of Lighthill's analogy proceed along similar lines and involve similar steps. Both formulations are exact and contain no approximation.

The starting point is however different in both cases. Curle's analogy is derived from an integral equation while Eq. (33) is derived by applying a weighted residual procedure to Lighthill equation. These two different starting points also correspond to two different classes of numerical methods: integral (or boundary element) method and finite element method, respectively. Consequently, Curle's analogy is the natural starting point for an implementation in a boundary element method, whereas the variational formulation of Lighthill's analogy is the natural starting point for finite element methods.

Curle's analogy clearly highlights the distinct roles of the bulk of the fluid (volume integral of quadrupole distribution), that of solid (*i.e.*, non-porous) boundaries (surface integral of dipole distribution), and that of control surfaces (*i.e.*, porous boundaries) on the aerodynamic sound. In contrast, the variational formulation of Lighthill's analogy does not separate the different contributions.

The treatment of the solid surfaces is however different in the two methods. On the one hand, Curle's analogy, Eq. (12) or (14), is purely explicit and uses the free field Green's function. Reflection of the aerodynamic sound by solid surfaces must be accounted for by the surface source terms. On the other hand,

the variational formulation of Lighthill's analogy is implicit and its practical use requires a discretization followed by the resolution of a system of equations (finite element method). The interactions between the solid surfaces and the aerodynamic sound are accounted for by the acoustic solver. If these effects are significant (*e.g.* for non-compact solid boundaries, see Caro³ *et al.*, and for interior/ducted aeroacoustic problems, see Section VI), this can be a crucial advantage of the variational formulation of Lighthill's analogy over Curle's analogy. The reason is that source terms are usually obtained from a CFD simulation that does not represent acoustic pressure fluctuations accurately enough to handle the various reflections.

E. Harmonic perturbations

The implementation of the variational formulation of Lighthill's analogy uses a frequency-domain formulation. Harmonic perturbations are considered, such that any perturbed quantity p can be written:

$$p(\mathbf{x}, t) = \text{Re}(\tilde{p}(\mathbf{x}) e^{i\omega t}). \quad (22)$$

Lighthill's equation Eq. (6) can be rewritten

$$\frac{\partial^2 \tilde{\rho}_a}{\partial x_i \partial x_i} + k^2 \tilde{\rho}_a = -\frac{1}{a_0^2} \frac{\partial^2 \tilde{T}_{ij}}{\partial x_i \partial x_j}, \quad (23)$$

where $k = \omega/a_0$ is the acoustic wavenumber. The weak variational statement associated to Eq. (23) is

$$\int_{\Omega} \left(k^2 \tilde{\rho}_a \delta \rho - \frac{\partial \tilde{\rho}_a}{\partial x_i} \frac{\partial \delta \rho}{\partial x_i} \right) d\mathbf{x} = \int_{\Omega} \frac{1}{a_0^2} \frac{\partial \tilde{T}_{ij}}{\partial x_j} \frac{\partial \delta \rho}{\partial x_i} d\mathbf{x} - \int_{\Gamma} \frac{\partial \tilde{\Sigma}_{ij}}{\partial x_j} n_i \delta \rho d\mathbf{x}. \quad (24)$$

In practice, if a CFD simulation is used to compute \mathbf{T} and $\mathbf{\Sigma}$, the derivative $\partial \tilde{T}_{ij}/\partial x_j$ are best computed by the CFD code on the CFD mesh. The reason is that the CFD mesh is usually finer than the acoustic mesh, which leads to a better approximation of derivatives. Moreover, this reduces the amount of data to exchange by a factor of 2. The complex vector $\widetilde{\text{divT}}$ is defined, in the frequency domain, for each node of the acoustic mesh:

$$\widetilde{\text{divT}}_i = \frac{\partial \tilde{T}_{ij}}{\partial x_j}. \quad (25)$$

Similarly, the complex vector $\widetilde{\text{divts}}$ is defined, in the frequency domain, for each node of the acoustic mesh on a control surface:

$$\widetilde{\text{divts}}_i = \frac{\partial \tilde{\Sigma}_{ij}}{\partial x_j}. \quad (26)$$

F. Treatment of boundary conditions

1. Solid boundaries

If the surface Γ is fixed or vibrating in its own plane, then $-n_i \frac{\partial}{\partial t} (\rho v_i)$ reduces to zero and the right-hand side of Eq. (24) vanishes. This corresponds to the *natural boundary condition* associated with the weak variational problem. This boundary condition must be applied on the solid boundaries that are in contact with the region where aeroacoustic sources are defined (see Figure 1).

2. Control surface

Consider a blower with its rotating part, as shown in Figure 1. A frequency-domain based acoustic code cannot use a mesh with sliding parts. Consequently, one has to enclose the rotating parts inside a *control surface*. Aerodynamic sources are defined on this surface, and account for the effect, on the noise generation, of the flow enclosed inside the control surface. Such a control surface is also termed a *porous boundary condition*. If the aerodynamic sources vanish, the control surface reduces to a solid boundary (*i.e.*, a reflecting boundary if there are no aerodynamic sources defined in the volume).

The CFD code must be able to output the quantity $\partial \Sigma_{ij}/\partial x_j$ on the control surface, so that ACTRAN can compute the right-hand side of Eq. (24).

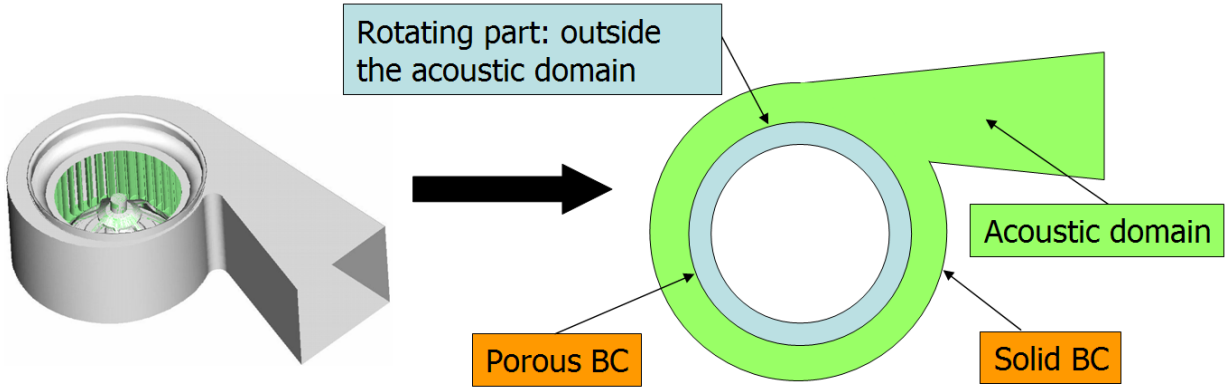


Figure 1. Use of solid and porous boundary conditions (control surface) for simulating the noise of a blower.

3. Infinite elements for radiation boundary condition

For applications to external aeroacoustic problems, the physical domain is unbounded and the pressure fluctuations must satisfy the Sommerfeld radiation condition at large distance from the aeroacoustic sources. This is enforced through the use of infinite elements. They are based on the multipole expansion of the solution of the wave equation. The order of the expansion directly governs the accuracy of the boundary condition. The infinite element method implemented in ACTRAN is an extension of a variable order Legendre polynomial formulation whose numerical performance has been extensively studied (Astley and Coyette^{12,13}). More details on the numerical implementation can be found in the ACTRAN User's manual.⁶

G. Application on a simple example

To validate our implementation on a simple flow, we consider small perturbations in a fluid at rest, so that

$$p = p_0 + (p - p_0) \quad (27)$$

$$\rho = \rho_0 + (\rho - \rho_0) , \quad (28)$$

where the 0 index denotes the corresponding quantities at rest, and

$$(p - p_0) \ll p_0 \quad (29)$$

$$(\rho - \rho_0) \ll \rho_0 . \quad (30)$$

To the first order in the fluctuations, Σ_{ij} in the surface source term of Eq. (24) becomes

$$\frac{\partial \Sigma_{ij}}{\partial x_j} = \frac{\partial p}{\partial x_i} . \quad (31)$$

Using the pressure gradient as a source term, we can validate our implementation with the solution of a simple acoustic problem.

Let us consider a dipole of strength D , centered at $\mathbf{x} = \mathbf{0}$, and aligned with the direction vector \mathbf{e}_x . The resulting pressure field at position \mathbf{x} is given by

$$p = i\rho_0\omega D \frac{x(1 + ikr) \exp(-ikr)}{4\pi|\mathbf{x}|^3} . \quad (32)$$

We can now validate our implementation using this simple solution. We enclose a dipole inside a spherical control surface, on which we apply a boundary condition based on Eq. (32). The finite element mesh is made of one layer of linear finite elements connected to infinite elements of order 10. Figure 2 shows a cut-away of the finite element mesh. The inner radius is 0.1, the outer radius is 0.15.

Figure 3 shows the comparison between the ACTRAN/LA simulation of the dipole radiation, and the analytical result as given by Eq. (32), for two different locations. All results correspond to $D = 1 \text{ m}^4/\text{s}$, $\rho_0 = 1.225 \text{ kg/m}^3$, and $a_0 = 340 \text{ m/s}$ in Eq. (32). The good agreement validates the implementation.

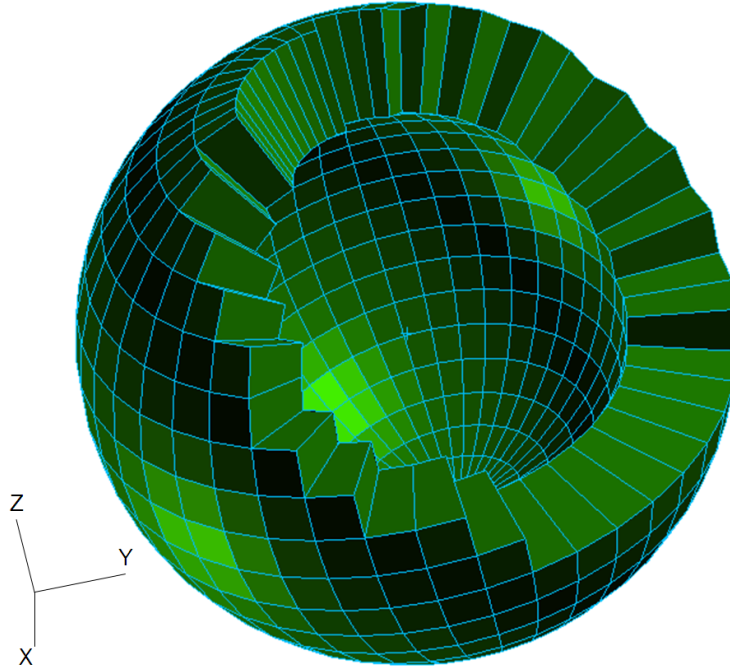


Figure 2. Cut-away of the finite element mesh used for simulating the radiation of a dipole.

III. The finite element method for the Navier-Stokes equations

The finite element weighted residual formulation of the Navier-Stokes equations¹⁴ may be stated as: Find solution $\{\mathbf{u}, p\} \in \mathcal{S}^h$ such that for all $\{\mathbf{w}, q\} \in \mathcal{V}^h$ the following equation is satisfied:

$$\begin{aligned}
& \int_{\Omega} w_i \left(\rho \frac{\partial v_i}{\partial t} + \rho v_j \frac{\partial v_i}{\partial x_j} - \rho b_i \right) - \frac{\partial w_i}{\partial x_i} p + \frac{\partial w_i}{\partial x_j} \tau_{ij} \, d\Omega \\
& + \int_{\Omega} q \frac{\partial \rho}{\partial t} - \frac{\partial q}{\partial x_i} \rho v_i \, d\Omega \\
& + \sum_e \int_{\Omega_e} \left(\rho v_j \frac{\partial w_i}{\partial x_j} + \rho \frac{\partial q}{\partial x_i} \right) \tau_m \left(\rho \frac{\partial v_i}{\partial t} + \rho v_k \frac{\partial v_i}{\partial x_k} + \frac{\partial p}{\partial x_i} - \frac{\partial \tau_{ik}}{\partial x_k} - \rho b_i \right) \, d\Omega \\
& + \sum_e \int_{\Omega_e} \frac{\partial w_i}{\partial x_i} \tau_c \left(\frac{\partial \rho}{\partial t} + \frac{\partial \rho v_j}{\partial x_j} \right) \, d\Omega \\
& = - \int_{\Gamma} (w_i h_i + q \dot{m}) \, d\Gamma
\end{aligned} \tag{33}$$

where \mathbf{b} is the body force; $\mathbf{w} = \{w_1, w_2, w_3\}^T$ and q are the weighting-function counterparts to \mathbf{u} and p , respectively; \mathcal{S}^h and \mathcal{V}^h are the finite element spaces of interpolations for the trial solution and weighting functions; Ω is the computational domain, with boundary Γ ; Ω_e is the element e domain; τ_m is the least-squares metric for the momentum equation, and τ_c is a least-squares continuity metric (see¹⁵ and references therein for additional details); $\mathbf{n} = \{n_1, n_2, n_3\}^T$ is the outward normal to the boundary; and $\dot{m} = \rho \mathbf{u}_n = \rho u_i n_i$ is the volumetric flow rate boundary condition.

In this analysis, we consider three variations of the Navier-Stokes equations, i) incompressible flow, where we set the density ρ to a constant, and the acoustic wave speed is infinite in the CFD computation, ii) pseudo compressible flow, where small density variations are accounted for in the continuity equation, and the acoustic wave speed is set to a_0 , iii) isentropic flow, where the density is a function of pressure only,

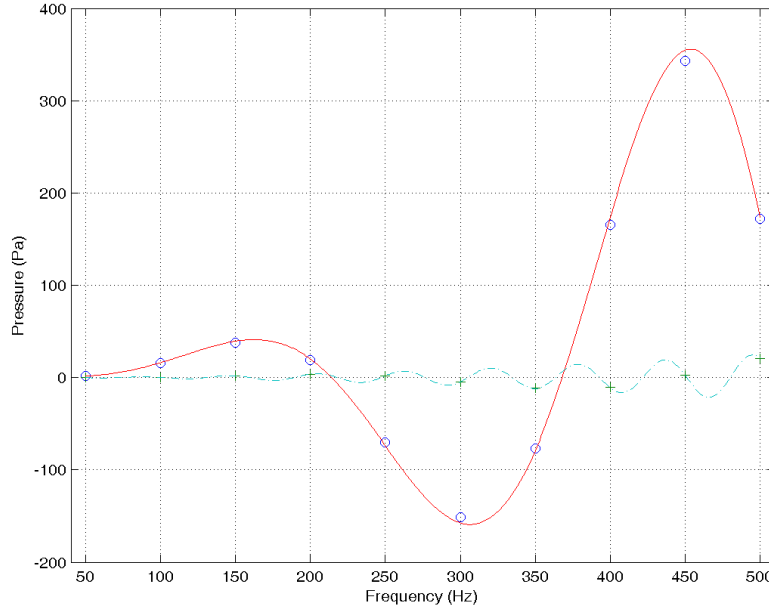


Figure 3. Comparison of analytical and numerical predictions for the radiation of a unit strength dipole. Real part of pressure fluctuation (Pa) as a function of frequency (Hz). Analytical solution at $(0.2, 0.5, 1)$ (solid), numerical solution at $(0.2, 0.5, 1)$ (\circ), analytical solution at $(0.3, 5, -3)$ (dotted-dashed), numerical solution at $(0.3, 5, -3)$ ($+$).

$\rho = \rho(p)$, given by the isentropic relation $\frac{p}{\rho_0} = \left(\frac{\rho}{\rho_0}\right)^\gamma$, and the acoustic waves propagate at the proper sound speed, a_0 . In the cases of incompressible flow and pseudo-compressible flow, the relation for the Lighthill's tensor simplifies to $T_{ij} = \rho v_i v_j - \tau_{ij}$.

Moreover, the equations are modified to account for the detached eddy simulation (DES) approach.¹⁶

IV. Coupling between ACUSOLVE and ACTRAN/LA

The coupling between ACUSOLVE and ACTRAN/LA relies on the exchange of data files written in the HDF format.¹⁷ The rationale for using the HDF format is that the resulting files are binary (hence size-efficient), portable, and can be read by many commercial software packages (such as Matlab, for example). In practice, ACUSOLVE produces HDF files that contain the values of $\overline{\mathbf{div}\mathbf{T}}$ and $\overline{\mathbf{div}\mathbf{t}}$ for different time steps. A utility from the ACTRAN/LA distribution, called I-LA, transforms these aerodynamic source terms from the time domain to the frequency domain. This results in another set of HDF files that are read directly by ACTRAN/LA.

V. Simulation-based design

To use simulations efficiently in a design process in the industry, it is important that CAE models can be built quickly. Since most air handling components are designed using a Computer Aided Design (CAD) system, interoperability between CAD and CAE is important. Computer simulations will increasingly be more important in a design process in the future because physical testing will remain costly, while computer simulations will be able to handle more and more complex physics and will get cheaper as hardware costs go down. If computer simulations are the primary means to evaluate the performance of an air handling system in the design process, the design process can be labelled as Simulation Based Design (SBD). To be efficient, SBD requires that the CAD and CAE be fully integrated. An important purpose of this work is to ensure that the predictions of noise levels can be performed within an SBD framework, for air handling

system development.

In this work, the geometrical models of the air handling blower are created in Pro/E. The framework to assign simulation attributes and to mesh the models directly from the CAD tool, is provided by SimApps by Simmetrix Inc. The simulation CFD files are automatically created for ACUSOLVE, and we plan to also provide a similar automated process to generate the simulation files for ACTRAN/LA.

VI. Preliminary results on a blower problem

A. Experimental setup for the acoustics measurements

The prototype blower scroll assembly used for the NVH test is made out of PMMA to provide a convenient optical access. In the NVH test set-up, the blower is elastically supported on rubber strings for isolation purposes. The blower axes is extended to minimize the influence of blower motor vibration on the measurement. Special attention was paid to ensure a smooth flow path; the number of obstacles like clips, screws etc. was kept to the absolute minimum. The housing of the scroll was reinforced and prepared to avoid resonances and structure born noise influencing the sound pressure measurements. A semi-anechoic room is used for the sound pressure level measurements. Background sound pressure level is below 15 dB(A), cut-off frequency is 50 Hz. The blower is positioned 1m from the floor on a stand. There are no obstructions close to the inlet or outlet of the scroll, ensuring an undisturbed in- and outflow. The blower speed was adjusted to 1500rpm (or $25\frac{rev}{s}$). Four B&K 4890 microphones were used to measure the sound pressure level. One microphone is located upstream of the inlet, and three downstream of the outlet, see Figure 4. Postprocessing was done using SQLab2 equipment and HEAD Artemis software.

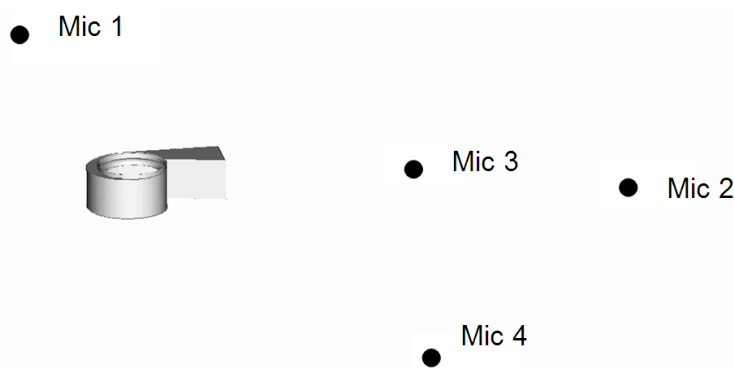


Figure 4. Experimental setup for sound measurements.

B. Flow field validation

The initial CFD simulations were carried out using a control volume similar to that used to measure the flow rates in a physical experiment. The outlet of the blower scroll was attached to a large box with a small outlet, which could be adjusted for different flow restrictions and back pressure, see Figure 5. In the present study, the opening was fully open, which implied that the resistance was very low. Note that the control volume for the flow rate evaluation is somewhat different than that used for acoustic evaluation. The acoustic test setup lacks the box attached to the scroll outlet, so that no adjustments for flow resistance can be made. We have performed CFD for both kinds of test setup, but the flow rate comparison can only be made on the test setup with the box attached to the scroll outlet. We ran CFD on different meshes, and we can not claim mesh-independent results. This is common for DES and LES type simulations. The flow rate variation is shown below in Table 1. More details about the mesh can be found in.⁵ A center plane with the velocity magnitude is shown in Figure 6. More plots can be found in.⁵

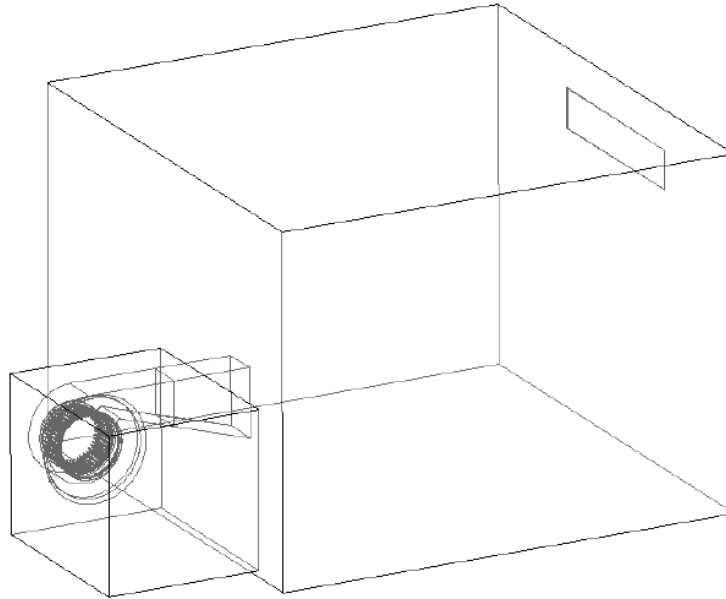


Figure 5. Experimental setup for flow rate measurements.

Model # elements	Flow rate [$\frac{kg}{s}$]	Flow rate [$\frac{l}{s}$]
9.1 M	0.168	136.9
18.5 M	0.175	142.9
31.0 M	0.181	147.4
Experiment		142.8

Table 1. Average flow rate for DES simulations compared the experimental flow rate.

C. Preliminary results

A first aeroacoustic prediction was made, using coarse meshes for both the CFD and the CAA. This resulted in an over prediction of sound pressure levels, when compared to the experiments. Consequently, a second run using a finer acoustic mesh in the boundary layers - in order to better capture the aerodynamic sources - was started. Early results indicate a dramatic improvement. At the time of this writing, however, we do not have long enough samples of results to start doing aeroacoustic predictions. Such predictions, together with a comparison with measurements, will be presented in a later publication. Figure 7 shows a snapshot of the divergence of Lighthill's tensor - the aerodynamic volume source - in the CFD domain.

VII. Conclusions

We have presented a novel aeroacoustic approach for predicting the noise level generated by an automotive blower. It is based on a two steps procedure. In a first step, an unsteady pseudo-compressible flow is computed using ACUSOLVE. This first step serves to predict aerodynamic noise sources of noise. In a second step, an acoustic computation is made using ACTRAN/LA. The variational formulation of Lighthill's analogy has been extended to allow it to handle control surfaces, upon which aerodynamic sources are defined. This is a key ingredient for treating blower problems.

Experiments on a ventilating blower have been performed, and sound pressure levels have been measured at four locations. CFD simulations of the ventilating blower have been performed, and have shown that

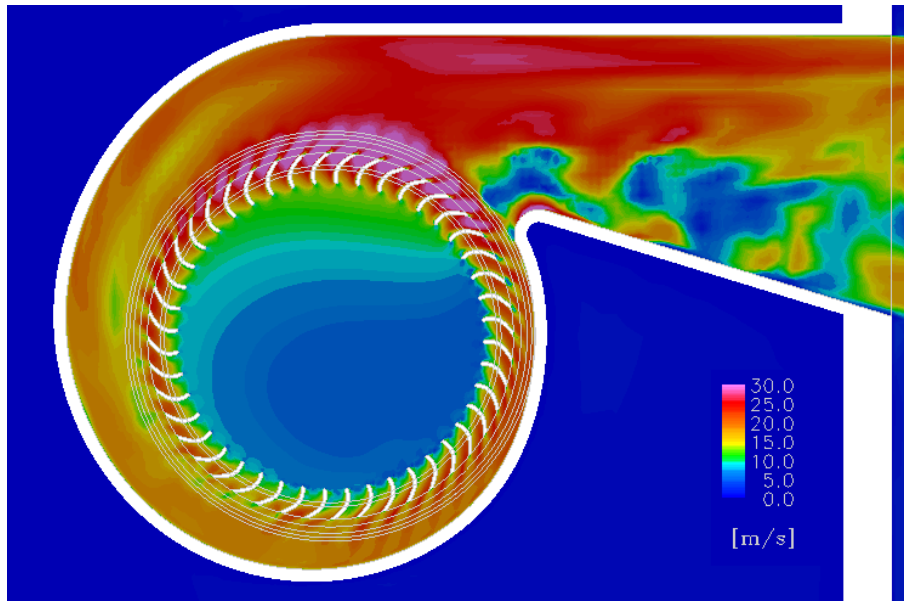


Figure 6. Snapshot of the magnitude of the velocity at a center cut of the blower.

ACUSOLVE can predict the flow rate inside the blower.

Future work include continuing higher-resolution computation, for both CFD and CAA, and comparing the predictions with experimental results. It might also be of interest to investigate possible improvements to the way aerodynamic sources are imported into ACTRAN/LA, to make the import less sensitive to the resolution of the acoustic mesh. It might be possible to take advantage of the fact that both ACUSOLVE and ACTRAN/LA are based on a finite element method to develop such an improved coupling approach.

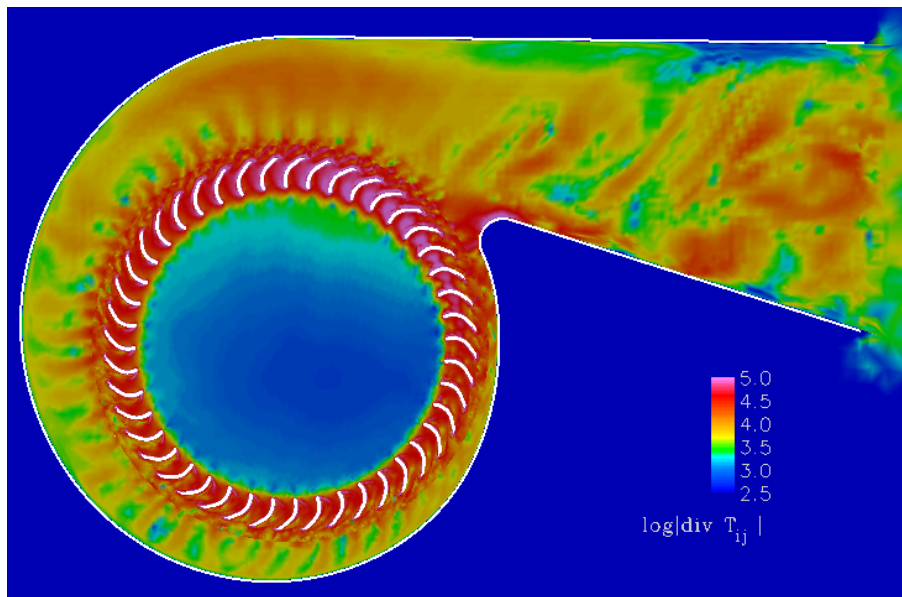


Figure 7. Snapshot of the divergence of Lighthill's tensor in the blower.

References

- ¹Oberai, A., Ronaldkin, F., and Hughes, T., "Computational Procedures for Determining Structural-Acoustic Response due to Hydrodynamic Sources," *Comput. Methods Appl. Mech. Engrg.*, Vol. 190, 2000, pp. 345–361.
- ²Oberai, A., Ronaldkin, F., and Hughes, T., "Computation of Trailing-Edge Noise due to Turbulent Flow over an Airfoil," *AIAA Journal*, Vol. 40, 2002, pp. 2206–2216.
- ³Caro, S., Ploumhans, P., and Gallez, X., "Implementation of Lighthill's Acoustic Analogy in a Finite/Infinite Elements Framework," AIAA Paper 2004-2891, 10th AIAA/CEAS Aeroacoustics Conference and Exhibit, 10-12 May 2004, Manchester, UK.
- ⁴ACUSIM-Software, I., *AcuSolve Command Reference Manual*, 2685 Marine Way, Suite 1215, Mountain View, California 94043, 2004.
- ⁵Sandboge, R., "CFD Analysis for a centrifugal benchmark blower with flat hub 1: Flow structures and noise source generation," Internal report.
- ⁶Free-Field-Technologies-S.A., *Actran 2004 Aeroacoustic Solutions: Actran/TM and Actran/LA - User's Manual*, 16, place de l'Université, 1348 Louvain-la-Neuve, Belgium, 2004.
- ⁷Lighthill, M., "On Sound Generated Aerodynamically," *Proc. Roy. Soc. (London)*, Vol. A 211, 1952.
- ⁸Goldstein, M., *Aeroacoustics*, McGraw-Hill, 1976.
- ⁹Jacob, M., "A Rod-Airfoil Experiment as Benchmark for Broadband Noise Modeling," *SWING Aeroacoustics Workshop, Stuttgart*, 2002.
- ¹⁰Curle, N., "The influence of Solid Boundaries on Aerodynamic Sound," *Proc. Roy. Soc. (London)*, Vol. A 231, 1955, pp. 505–514.
- ¹¹Stratton, J., *Electromagnetic Theory*, NY - Mc Graw Hill, 1941.
- ¹²Astley, R. and Coyette, J., "Conditioning of infinite element schemes for wave problems," *Commun. Numer. Meth. Engrg.*, Vol. 17, 2001, pp. 31–41.
- ¹³Astley, R. and Coyette, J., "The performance of spheroidal infinite elements," *International Journal for Numerical Methods in Engineering*, Vol. 52, 2001, pp. 1379–1396.
- ¹⁴Brooks, A. and Hughes, T., "Streamline Upwind/Petrov-Galerkin Formulations for Convection Dominated Flows with Particular Emphasis on the Incompressible Navier-Stokes Equations," *Comput. Methods Appl. Mech. Engrg.*, Vol. 32, 1982, pp. 199–259.
- ¹⁵Hughes, T., "Recent Progress in the Development and Understanding of SUPG Methods with Special Reference to the Compressible Euler and Navier-Stokes Equations," *International Journal for Numerical Methods in Engineering*, Vol. 7, 1987, pp. 1261–1275.
- ¹⁶ASME, P. F., editor, *Computational Fluid Dynamics Model for Tacoma Narrows Bridge Upgrade Project*, No. FEDSM2003-45514, 2003.
- ¹⁷"HDF file format," <http://hdf.ncsa.uiuc.edu/>.